Energy & Buildings 347 (2025) 116255

Contents lists available at ScienceDirect

Energy & Buildings

journal homepage: www.elsevier.com/locate/enb

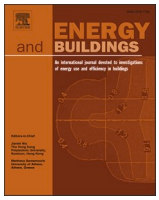

MLGA-GNN: Assessing horizontal and vertical heterogeneity in the photovoltaic potential of urban-scale building facades

Zheng Li [a], Jun Ma [a,b,*], Waishan Qiu [a], Xiao Li [c], Feifeng Jiang [a]

[a] Department of Urban Planning and Design, The University of Hong Kong, Hong Kong, China
[b] Urban Systems Institute, The University of Hong Kong, Hong Kong, China
[c] Department of Civil Engineering, The University of Hong Kong, Hong Kong, China

ARTICLE INFO

Keywords:
Photovoltaic potential assessment
building facade
graph neural networks
machine learning
solar radiation intensity

ABSTRACT

Assessing the photovoltaic (PV) potential of urban building facades is crucial for achieving urban energy transition and carbon reduction goals. However, traditional assessment methods overlook the vertical variation of solar radiation intensity (SRI) on building facades, potentially underestimating the PV potential of local areas. This study proposes a novel method that vertically divides building facades into layers and predicts the solar radiation intensity (SRI) of each layer to evaluate the PV potential of building facades. Taking New York City as a case study, our results show that the proposed Multi-Layer Geo-Attention Graph Neural Network (MLGA-GNN) achieves better prediction performance than traditional machine learning and deep learning models. The spatial distribution of SRI shows lower values in dense, high-rise city centers due to shading effects, and higher values in peripheral areas with shorter, more spaced buildings. In the vertical direction, the SRI increases with height, forming a clear upward trend along with building elevations. Further analysis reveals that the MLGA-GNN can uncover significant differences in SRI between the top and bottom layers of buildings, helping to identify local high-irradiance areas overlooked by traditional assessment methods. Moreover, economic benefit and carbon reduction analyses based on different investment payback periods indicate that a 10–15-year payback period achieves a good balance between returns and costs. This research enriches the methods for assessing the PV potential of buildings at an urban scale, and provides decision support for the macro-layout and micro-design of urban PV systems.

1. Introduction

1.1. Background

In the context of escalating global climate change and the growing energy crisis, seeking sustainable energy solutions has become a crucial agenda for the international community. According to a report by the United Nations Environment Programme (UNEP) [1], in 2022, the global building sector consumed approximately 34 % of energy and generated about 37 % of carbon emissions, making it one of the major contributors to energy consumption and greenhouse gas emissions. To achieve the global goals of “carbon peaking” and “carbon neutrality,” the low-carbon transformation of the building sector is particularly important [2].

As a clean and renewable energy solution, solar photovoltaic (PV) technology has shown immense potential for application in the building sector [3,4]. Building-integrated photovoltaic (BIPV) systems can not only utilize solar energy resources for distributed power generation on-site but also effectively reduce buildings’ dependence on traditional fossil fuels. Research has demonstrated that the large-scale application of BIPV systems can significantly reduce carbon emissions during the operational phase of buildings, making a substantial contribution to achieving sustainable urban development and tackling climate change [5].

BIPV systems can be broadly classified into two categories based on their installation locations: rooftop PV systems and facade PV systems [6]. Rooftop PV systems are currently the most widely used form, where solar panels are installed on building rooftops, utilizing the rooftop space for power generation. This installation method is simple, does not occupy additional land resources, and does not affect the main structure and appearance of buildings. Rooftop PV systems are suitable for various types of buildings, such as residential, commercial, and industrial

* Corresponding author at: Urban Systems Institute, The University of Hong Kong, Pokfulam Road, Hong Kong, China.
E-mail address: junma@hku.hk (J. Ma).

https://doi.org/10.1016/j.enbuild.2025.116255
Received 30 June 2025; Received in revised form 24 July 2025; Accepted 4 August 2025
Available online 6 August 2025

buildings, showing broad application prospects. In contrast, facade PV systems integrate solar panels into the exterior walls of buildings, forming an integrated building PV curtain wall. This approach not only generates electricity but can also serve as a decorative material for the building facade, enhancing the aesthetic value of the building.

While building rooftops are ideal locations for installing photovoltaic systems, primarily due to their superior solar radiation reception conditions and minimal shading effects, their limited installation area can hardly support the electrical energy demand of an entire building, especially for commercial or high-rise buildings [7–9]. In contrast, building facades offer a much broader application space for photovoltaics. According to the research by Esclapes et al. [10], in urban environments, building facade areas account for approximately 60 %–80 % of the total building surface area, indicating that building facades have enormous potential for PV power generation. This significant area advantage not only compensates for the insufficiency of rooftop areas but also enables buildings to have larger-scale solar energy production capabilities.

However, due to the complexity of the urban environment, accurately assessing the PV power generation potential of building facades still faces significant challenges. This assessment must consider multiple factors, including building geometry, surrounding shading effects, solar radiation conditions, and interaction among building groups. Traditional assessment methods often struggle to effectively handle these complex spatial relationships, leading to limitations in the accuracy and reliability of the prediction results. Therefore, developing more precise and efficient prediction methods is of great practical significance for promoting the large-scale application of BIPV systems.

1.2. Literature review

To systematically examine the current research status and progress in building PV potential prediction, this section reviews research on both building rooftops and facades.

1.2.1. Rooftop photovoltaic potential prediction

Rooftops have long been recognized as the predominant location for the deployment of BIPV systems, primarily due to their advantageous solar exposure, relatively unobstructed spatial conditions, and ease of installation and maintenance [11]. These characteristics make rooftops an ideal platform for harnessing solar energy in urban environments, especially within the constraints of high-density development. As the global emphasis on renewable energy intensifies, accurate assessment of rooftop PV potential has become a critical step in optimizing urban solar energy strategies [12].

Over the past decade, driven by rapid advancements in data acquisition technologies and computational methods, the assessment techniques for rooftop PV potential have evolved significantly. Early-stage research primarily relied on geographic information systems (GIS), remote sensing, and rule-based estimation models [13–15]. However, recent developments in artificial intelligence (AI), machine learning, and deep learning have led to the emergence of intelligent, high-resolution prediction frameworks capable of handling large-scale urban datasets with greater accuracy and efficiency. This methodological shift has not only improved the precision of rooftop PV assessments but also expanded their applicability across diverse urban morphologies and climatic conditions.

Early studies mainly relied on GIS and remote sensing technologies for rooftop PV potential assessment [16–18]. Singh et al. [19], using Mumbai, India, as an example, established a comprehensive framework for regional-scale rooftop PV potential assessment by integrating public data, GIS analysis, and PVSyst simulation. The study not only considered basic parameters such as building footprint ratio and available rooftop area ratio but also incorporated environmental factors like irradiance, temperature, and tilt angle into the assessment system. The results showed that Mumbai's PV installation potential reached 2190 MW, with a capacity factor of 14.8 %, capable of meeting 12.8–20 % of the daily average electricity demand and 31–60 % of the early peak demand, providing significant insights for urban energy planning.

With the rapid development of big data and artificial intelligence technologies, a new generation of rooftop PV potential prediction methods has emerged [20–22]. Zhong et al. [23] proposed an innovative assessment framework based on deep learning, which has the following features: developing a deep learning-based automatic rooftop area identification algorithm for feature extraction; significantly reducing training data preparation costs (by approximately 80 %) through a spatial optimization sampling strategy; and precisely assessing the total rooftop area (330.36 square kilometers) and potential installed capacity (66 GW) in Nanjing, China, with an annual power generation potential of 49,897 GWh.

In summary, research on rooftop PV potential prediction has formed a relatively comprehensive technical system. From a methodological perspective, the research has evolved from traditional GIS and remote sensing techniques to intelligent methods such as machine learning and deep learning, with assessment tools becoming more diverse and precise. Particularly in recent years, the introduction of artificial intelligence technologies has provided new solutions for addressing key issues such as data acquisition, feature extraction, and model optimization. However, compared to building facade PV potential prediction, rooftop PV assessment has natural advantages such as relatively easy data acquisition and fewer shading effects, which are important reasons for the rapid development of research in this field. These research findings not only provide a reliable theoretical basis for the planning and design of rooftop PV systems but also offer valuable methodological references for subsequent research on building facade PV potential prediction.

1.2.2. Facade photovoltaic potential prediction

Compared to rooftop PV systems, the potential prediction of facade PV systems has received relatively less attention [24]. However, with the development of BIPV technology and the intensifying trend of urban densification, facade PV systems show broad application prospects [25]. In recent years, an increasing number of studies have focused on facade PV potential prediction and have proposed various novel methods and techniques [26–28].

Simulation based on three-dimensional (3D) building models is currently one of the main methods for assessing the power generation potential of facade PV systems [29]. Brito et al. [30] conducted an in-depth study of typical cases in Lisbon, Portugal, using digital surface models obtained from LiDAR measurements and typical meteorological year data. The study showed that PV systems combining rooftops and facades could meet 50–75 % of the total electricity demand, with facade PVs playing a significant role in satisfying winter electricity needs. From an economic perspective, the payback period for pure rooftop schemes can be less than 10 years, while the payback period for balanced rooftop and facade configuration schemes is approximately 15 years. In the field of rural buildings, Liu et al. [31] proposed an innovative evaluation method that constructs rural 3D building models through publicly available satellite images and vector maps for the first time, achieving precise evaluation of the PV potential of rural buildings. The method was validated by field solar radiation measurements, and the study found that south- and north-facing rooftops, as well as south- and west-facing facades, exhibited the highest PV potential. In particular, north-facing rooftops with a 30° inclination account for 32.7 % of the total rooftop PV potential, highlighting the importance of not overlooking the potential contribution of specific building surface orientations.

To understand the factors influencing facade PV potential, Tao et al. [32] evaluated the impact of urban morphology parameters by establishing machine learning models. Taking high-rise, high-density urban areas in Hong Kong as an example, the study found that plot ratio, building floor, building density, and perimeter shape factor are the four most important parameters affecting facade PV potential. Furthermore, based on the shortest payback period and maximum power generation,

the study optimized the location, quantity, and transparency of BIPV. The results showed that when the surrounding building heights are lower, south-facing facades can achieve the optimal payback period and power generation. This study provides new ideas and methods for predicting the PV potential of building facades in high-density urban areas.

However, existing facade PV potential assessment methods still have significant limitations. The primary issue is the limitation of assessment accuracy. Most studies treat the entire facade as a homogeneous surface, overlooking the differences in solar radiation intensity (SRI) at different locations on the facade due to shading from surrounding buildings. This simplification may lead to biased assessment results, particularly for areas with locally high SRI, where the actual PV potential may be significantly underestimated. The second limitation is the research scale. Existing high-precision studies are mostly limited to individual buildings or small-scale areas, and their assessment methods and conclusions are difficult to generalize to the urban scale. This limitation poses significant obstacles to guiding the formulation of facade PV policies at the urban level and highlights the necessity of developing new assessment methods.

1.3. Objective, novelties, and contributions

To overcome the limitations of existing studies, this research proposes an innovative urban-scale building facade PV potential assessment method—Multi-Layer Geo-Attention Graph Neural Network (MLGA-GNN). The core innovation of this method lies in its ability to accurately assess the distribution of SRI at varying heights on building facades, thereby enabling a refined assessment of facade PV potential. Compared to traditional methods that simplify the entire facade, MLGA-GNN can effectively capture the SRI variations along the vertical direction of building facades through multi-layer modeling and geospatial attention mechanisms. This refined assessment method not only accurately identifies facade areas with higher PV potential but also provides a basis for optimizing the layout of PV systems. Particularly in high-density urban areas, where the building shading effect is significant and the SRI varies greatly across the facade, the MLGA-GNN provides important practical value. Furthermore, the assessment results of this method can directly guide the economic optimization of PV systems. By identifying high-efficiency areas on the facade, unnecessary investment costs can be reduced by avoiding the installation of PV modules in low SRI areas, thereby improving the overall economic benefits of the system. This feature has significant practical implications for the large-scale promotion of building facade PV systems.

2. Methodology

This study proposes a comprehensive framework for assessing the PV potential of urban building facades (Fig. 1). The study first integrates basic information such as building footprint contours, building heights, and meteorological data. These datasets are used to generate detailed 3D models of urban buildings, and solar radiation simulations are performed to obtain specific radiation values for each building. On this basis, the study further constructs building groups, identifies spatial relationships between target buildings and surrounding buildings, and extracts building graph features, laying the foundation for the subsequent application of deep learning models. In the model construction stage, the study employs an innovative MLGA-GNN method. This method first converts the extracted building features and solar radiation simulation results into structured graph data, then captures the complex spatial relationships and shading effects among building groups through model training. The study's outcomes include detailed PV potential analysis of facades, research on the façade heterogeneity in both horizontal and vertical directions, and comprehensive cost-benefit and carbon emission reduction analyses.

2.1. Study area and data collection

To verify the research framework, the study selects New York City (NYC) as the study area (Fig. 2). NYC has approximately 1.08 million buildings, providing an ample and diverse data foundation for model training and validation. As one of the most representative metropolises globally, NYC's built environment embodies the typical characteristics of modern urban development. From the dense high-rise commercial districts in Manhattan to the relatively low-density residential areas in Brooklyn, the significant differences in building heights, densities, and morphologies within the city provide an ideal testing scenario for the study, making the research results more widely applicable and valuable for reference. As a typical high-density city, NYC's building clusters

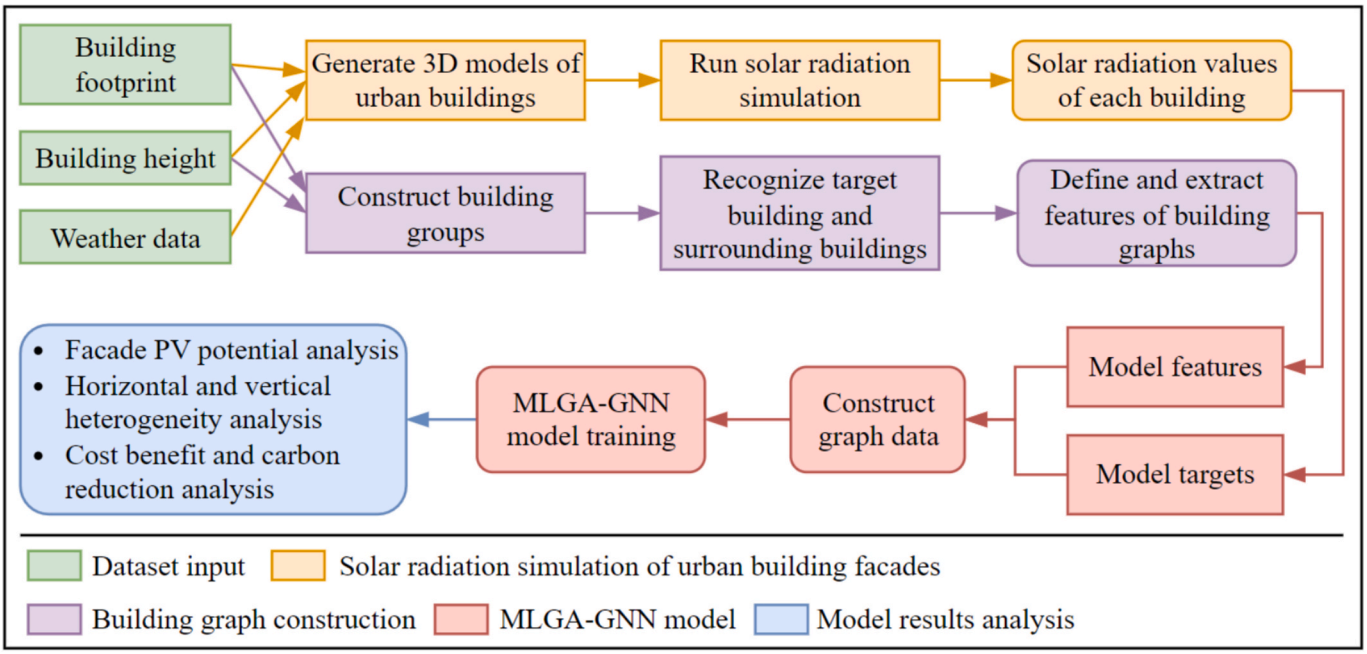

Fig. 1. The workflow of the study.

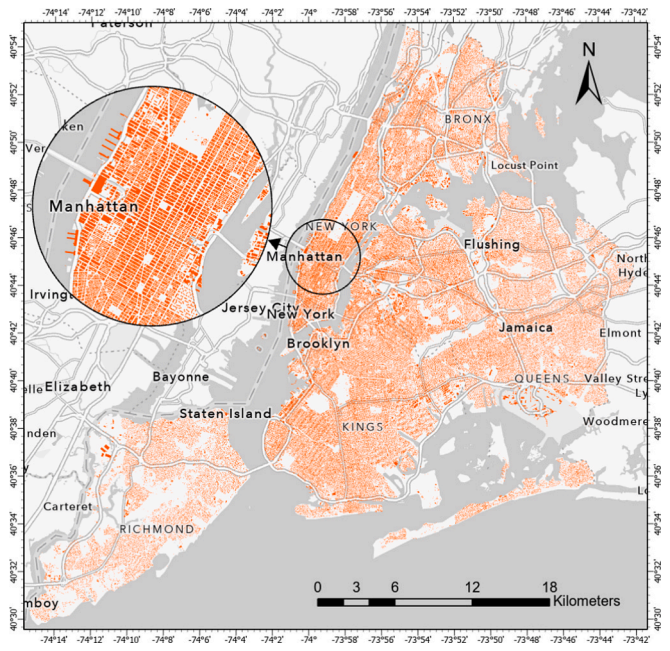

Fig. 2. The buildings in the study area.

exhibit a pronounced mutual shading effect, a complex spatial relationship that traditional facade PV assessment methods struggle to accurately address. This characteristic provides an ideal research environment to validate the advantages of the MLGA-GNN method in handling building shading effects. From the perspective of solar energy resources, NYC is located near 40°N latitude, with an average annual solar radiation of approximately 4.0–4.5 kWh/m^2/day, indicating a good potential for solar energy development.

Moreover, NYC's open data policy provides high-quality building geometry and attribute data for the study, which are crucial for method validation and promotion. All datasets in this study are sourced from NYC's open data website, which is freely accessible to all (Table 1).

2.2. Solar radiation simulation of building facades

Acquiring high-quality training data is a crucial step in model development for building facade PV potential prediction research. To train the MLGA-GNN model proposed in this study, we require a large amount of accurate SRI data for building facades. However, in real-world scenarios, directly measuring the SRI of each building facade in a large-scale urban environment is not only technically challenging but also requires substantial human and material resources, making it often impractical. To overcome this limitation, this study employs building solar radiation simulation methods to generate the necessary training data.

Table 1
The primary information of the datasets.

Index	Dataset	Source	Primary features	Samples	Data format
1	Building dataset	NYC open data (https://opendata.cityofnewyork.us/)	Building footprint, building height, geographic location, etc.	1,084,465 buildings	Shapefile (polygon)
2	Weather dataset	EPW Map (http://www.ladybug.tools/epwmap/)	Air temperature, relative humidity, global irradiance, wind speed, etc.	8760 h	GeoJSON

Among the various available solar radiation simulation tools, this study selects Ladybug Tools as the primary simulation platform [33]. This choice is based on several key advantages: firstly, Ladybug Tools can efficiently calculate solar radiation at different time steps, fully considering the dynamic changes in solar position angles; secondly, the tool can accurately simulate the shading effects between buildings in complex urban environments, which is particularly important for radiation assessment of high-density urban building clusters; lastly, it can generate detailed radiation distribution data for building surfaces, providing a reliable foundation for subsequent analysis. It is worth noting that Ladybug Tools has been validated and applied in numerous high-quality studies [34–36], and its simulation results have gained widespread recognition in the academic community.

The specific simulation process is shown in Fig. 3. First, Level of Detail-1 (LoD1) 3D models of all buildings in the study area are constructed using Rhino software. Then, the Ladybug Tools plugin is invoked in Grasshopper to perform solar radiation simulations. In this stage, we subdivide the building facades into 1-meter grid units and precisely calculate the SRI for each grid at different time points. This grid-based processing method ensures computational accuracy while reflecting the spatial heterogeneity of facade radiation distribution. Finally, the simulated radiation data is systematically organized to establish a structured dataset containing building IDs, grid IDs, timestamps, and corresponding solar radiation intensities. These data provide a solid foundation for subsequent model training.

2.3. Building graph construction

2.3.1. Building groups and graph data construction

In urban environments, the shading influence of buildings on surrounding structures rapidly diminishes as the distance increases. Based on this characteristic and relevant research findings, this study proposes a reasonable spatial influence range assumption: when the distance between surrounding buildings and the target building exceeds three times the height of the target building, the shading effect can be considered negligible [37,38]. This assumption not only helps simplify computational complexity but also aligns with the observed attenuation pattern of shading effects.

Based on this assumption, we define a unique group for each building. Specifically, for any target building, we only consider the surrounding buildings located within a radius of three times its height, with

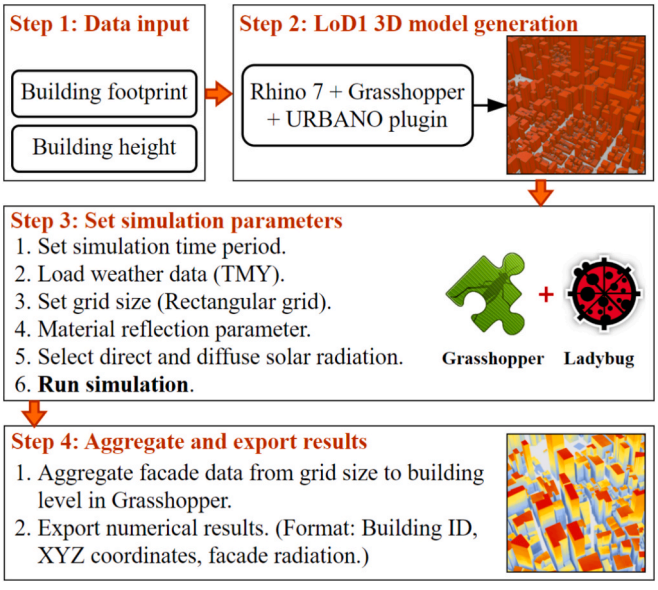

Fig. 3. The solar radiation simulation process.

the target building as the center. As shown in Fig. 4, a typical building group consists of a target building (marked in orange) and the surrounding buildings within its influence range (marked in blue). In this example, there are five buildings around the target building that fall within its influence range, collectively forming a complete building group. In a large urban environment like NYC, since the geometric characteristics such as height and location of each building vary, their corresponding influence ranges also change, allowing us to generate approximately 1.08 million unique building groups.

To convert these building groups into data structures suitable for graph neural network (GNN) processing, we further transform each building group into building graph data. In real urban environments, due to differences in building heights and volumes, the shading influence between buildings is directional: for example, the shading effect of high-rise buildings on low-rise buildings may be significant, while the influence of low-rise buildings on high-rise buildings is relatively small. However, to simplify computational complexity and improve the generalizability of the model, this study makes a simplifying assumption: all influence relationships between buildings are considered bidirectional, and therefore, undirected graphs are used to represent building graph data. This representation method establishes an undirected connection between the target building and each surrounding building within its influence range.

2.3.2. Graph features definition and selection

This study draws upon previous research on building geometric characteristics to define the node features and edge features of the graph data [39–41], which describe the individual attributes of buildings and the spatial relationships between them, respectively. However, directly using all possible geometric features may lead to information redundancy among the features, which not only increases computational complexity but also affects the predictive performance of the model. To address this issue, this study conducts a correlation analysis on all candidate features. By calculating the Pearson correlation coefficients between features and adopting a threshold of 0.7, the study selects a subset of features with low collinearity. This feature selection strategy ensures the information richness of the feature set while avoiding excessive redundancy among features. Table 2 provides a detailed list of the features that were selected and their main information.

2.4. MLGA-GNN model

2.4.1. Multi-layer division of building facades

In the assessment of PV potential on building facades, the spatial distribution of SRI is a key factor. Traditional methods often treat building facades as a whole, using a single average value to characterize their solar radiation properties [28,42]. However, due to the shading effects of surrounding buildings, building facades often exhibit significant gradients in SRI along the vertical direction. To more accurately capture this spatial heterogeneity, this study proposes a vertical multi-layer division approach.

This method is based on a simplifying assumption that all positions at the same vertical height on a building facade receive approximately the same Solar Radiation Intensity (SRI). While this assumption neglects potential local variations in the horizontal direction—such as differences caused by façade articulation or adjacent obstructions—it effectively captures the dominant vertical variation pattern and significantly reduces computational complexity while maintaining reliable accuracy.

As illustrated in Fig. 5, we uniformly divide each building facade into 10 vertical layers, with each layer representing approximately 10 % of

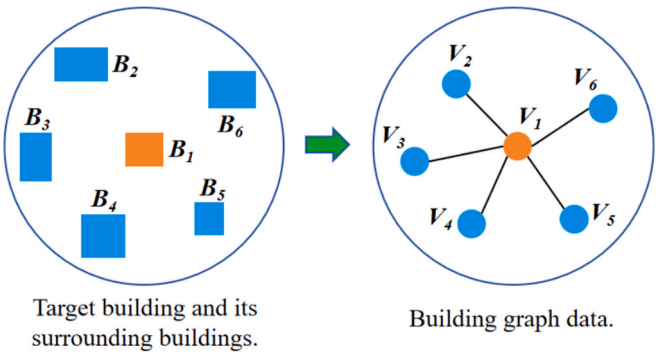

Fig. 4. Converting buildings into building graph data in a building group.

Table 2
The selected features.

Category	Features	Definition
Node features	Building height	The vertical distance from ground level to the highest point of the building (m).
	Building footprint area	The total ground area covered by the building (m^2).
	Building surface area	The total area of all external surfaces including walls and roof (m^2).
	Building volume	The total enclosed space within the building (m^3).
	Building shape coefficient	The ratio of building surface area to building volume (m^{-1}).
	Gross floor area	The sum of floor areas of all levels within the building (m^2).
	Built floor area ratio	The ratio of gross floor area to building footprint area.
	Year of alteration	The most recent year when significant modifications were made to the building.
	Average building height	The mean height of a building group (m).
	Building density	Number of buildings per unit area in the building group (buildings/m^2).
	Floor area ratio	The gross floor area is divided by the building footprint area.
	Normalized compactness index	The total floor area of all buildings in the building group.
	Volume area ratio	The building volume is divided by the building footprint area.
	Building coverage ratio	The total building footprint area is divided by the building group area.
	Building height distribution	The height of the target building is subtracted from the sum of the heights of all surrounding buildings in turn.
Edge features	Distance	Euclidean distance between centroids of two buildings (m).
	Azimuth	Horizontal angle between two buildings relative to true north (degrees).
	Elevation	Vertical angle between two buildings (degrees).

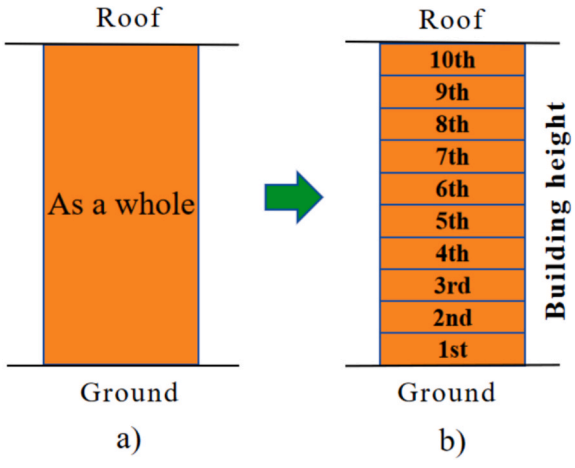

Fig. 5. Building facade: Split it into 10 layers according to building height. Traditional method (left), our method (right).

the total building height. Each layer corresponds to a single prediction point, reflecting the average SRI within that height range. The decision to use 10 layers balances spatial resolution with computational efficiency: it is fine enough to capture meaningful vertical changes in SRI, while avoiding excessive data volume or modeling complexity, which would arise from overly fine stratification—especially in large-scale urban simulations. This stratified modeling approach allows for a more detailed assessment of vertical SRI variation compared to traditional holistic façade modeling, thereby offering a more nuanced and practical basis for optimizing the vertical deployment of photovoltaic (PV) systems.

2.4.2. Geo-attention mechanism

Although basic GNN models can aggregate information from surrounding buildings to the target building, their simple information aggregation approach struggles to accurately reflect the complexity of inter-building influences in urban environments [43–45]. In real-world settings, the degree of influence exerted by surrounding buildings on the target building often varies due to their spatial positions and geometric characteristics. For instance, buildings that are closer in proximity, larger in volume, or taller in height typically generate more significant shading effects, while the influence of buildings that are farther away or smaller in volume is weaker.

To more accurately characterize this differentiated spatial influence, this study introduces the geo-attention mechanism. This mechanism achieves adaptive weighting of the influence of surrounding buildings by incorporating attention computation based on geospatial features. Specifically, the geo-attention mechanism utilizes the spatial relationships and geometric characteristics between buildings to calculate attention coefficients, thereby quantifying the degree of influence among different buildings. This enables the model to automatically identify and highlight surrounding buildings that have significant influence while appropriately reducing the weights of buildings with less impact. Through this differentiated weight assignment mechanism, the model can more precisely capture the complex spatial interactions within building clusters, thereby improving the accuracy of PV potential predictions. This approach not only enhances the expressive power of the model but also better aligns with the characteristics of inter-building influences in real urban environments.

Specifically, Equations (1) and (2) represent the basic attention mechanism, while Equations (3)-(5) represent the geo-attention mechanism proposed in this study.

$$e(\boldsymbol{h}_i, \boldsymbol{h}_j) = \mathrm{LeakyReLU}\left(\boldsymbol{a}^{\top} \cdot \left[\boldsymbol{W}\boldsymbol{h}_i \| \boldsymbol{W}\boldsymbol{h}_j\right]\right) \tag{1}$$

$$\alpha_{ij} = \mathrm{softmax}_j\left(e(\boldsymbol{h}_i, \boldsymbol{h}_j)\right) = \frac{\exp\left(\mathrm{LeakyReLU}\left(\boldsymbol{a}^{\top} \cdot \left[\boldsymbol{W}\boldsymbol{h}_i \| \boldsymbol{W}\boldsymbol{h}_j\right]\right)\right)}{\sum_{j' \in \mathcal{N}_i} \exp\left(\mathrm{LeakyReLU}\left(\boldsymbol{a}^{\top} \cdot \left[\boldsymbol{W}\boldsymbol{h}_i \| \boldsymbol{W}\boldsymbol{h}_{j'}\right]\right)\right)} \tag{2}$$

$$f(\boldsymbol{A}_{ij}) = \frac{1 - \cos(\boldsymbol{A}_{ij})}{2} \tag{3}$$

$$e'(\boldsymbol{h}_i, \boldsymbol{h}_j) = a^T \frac{f(A_{ij}) E_{ij}}{D_{ij}} \mathrm{LeakyReLU}\left(W\left[\mathbf{h}_i \| \mathbf{h}_j\right]\right) \tag{4}$$

$$\alpha'_{ij} = \mathrm{softmax}_j\left(e'(\boldsymbol{h}_i, \boldsymbol{h}_j)\right) = \frac{\exp\left(a^T \frac{f(A_{ij}) E_{ij}}{D_{ij}} \mathrm{LeakyReLU}\left(W\left[\mathbf{h}_i \| \mathbf{h}_j\right]\right)\right)}{\sum_{j' \in \mathcal{N}_i} \exp\left(a^T \frac{f(A_{ij}) E_{ij}}{D_{ij}} \mathrm{LeakyReLU}\left(W\left[\mathbf{h}_i \| \mathbf{h}_j\right]\right)\right)} \tag{5}$$

- $\boldsymbol{\alpha_{ij}}$ is the attentional weight of node $\boldsymbol{i}$ on its neighboring node $\boldsymbol{j}$, $\boldsymbol{W}$ is the weight matrix, $\boldsymbol{a}$ is the parameter vector used to compute the attentional coefficients, $\boldsymbol{h_i}$ and $\boldsymbol{h_j}$ are the feature vectors of the node, ***LeakyReLU*** is the activation function, and ***SoftMax*** is the normalization method.
- $\boldsymbol{A_{ij}}$ is the azimuth that is the angle between the line connecting $\boldsymbol{building_i}$ and $\boldsymbol{building_j}$ and the north direction, $\boldsymbol{E_{ij}}$ is the elevation between $\boldsymbol{building_i}$ and $\boldsymbol{building_j}$, $\boldsymbol{D_{ij}}$ is the distance between $\boldsymbol{building_i}$ and $\boldsymbol{building_j}$. When $\boldsymbol{i} = \boldsymbol{j}$, set $\boldsymbol{A_{ij}}$, $\boldsymbol{E_{ij}}$ and $\boldsymbol{D_{ij}}$ to 1. Fig. 6 briefly illustrates the relationship between $\boldsymbol{A_{ij}}$, $\boldsymbol{E_{ij}}$ and $\boldsymbol{D_{ij}}$.
- Equation (3) converts the angular values of azimuth into continuous numerical values with the same trend.

2.4.3. The workflow of MLGA-GNN

Fig. 7 illustrates the complete workflow of the MLGA-GNN model, encompassing the entire process from model input and training to final output. In the data preprocessing stage, the model first vertically divides the facade of each target building into 10 equal layers and constructs a graph data structure for each layer, establishing spatial associations with surrounding buildings. It is worth noting that during the graph data construction process, the height feature of each facade layer is updated to its actual height, rather than using the total building height, allowing for a more accurate representation of features at different height positions. The model takes node and edge features as input "X" and uses the solar radiation simulation values obtained from Section 2.2 as training labels "Y".

During the model training phase, MLGA-GNN first processes the input graph data through the geo-attention mechanism, computing and assigning spatial attention weights. Subsequently, the model performs feature extraction and information aggregation through multiple layers of GNNs, enabling it to fully learn the complex spatial interactions within building clusters. Finally, the model outputs corresponding prediction values for each facade layer, forming a complete vertical distribution of solar radiation on the building facade. This layer-based modeling strategy not only provides higher spatial resolution but also allows the model to more accurately capture variations characteristics of solar radiation on building facades.

Compared to conventional models such as regression or basic GNNs, the proposed MLGA-GNN better captures the vertical variation of solar radiation by dividing facades into layers, and improves prediction accuracy through a geo-attention mechanism that accounts for the spatial influence of surrounding buildings. While this approach increases model expressiveness, it also introduces additional computational cost and relies on the simplifying assumption of horizontal uniformity within each layer. Nonetheless, it offers a practical balance between accuracy and efficiency for large-scale urban PV potential assessment.

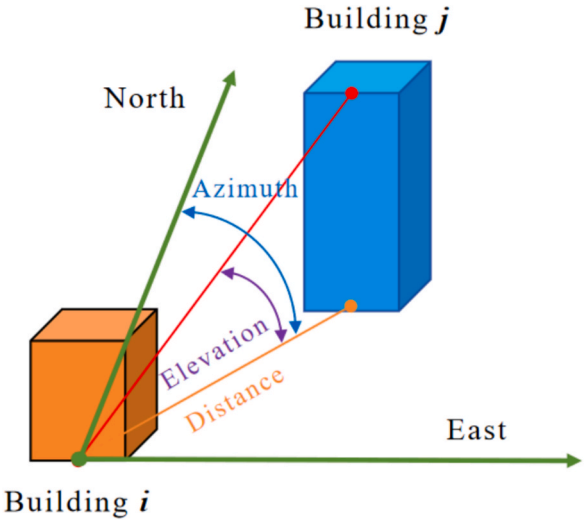

Fig. 6. The relationship between azimuth, elevation, and distance.

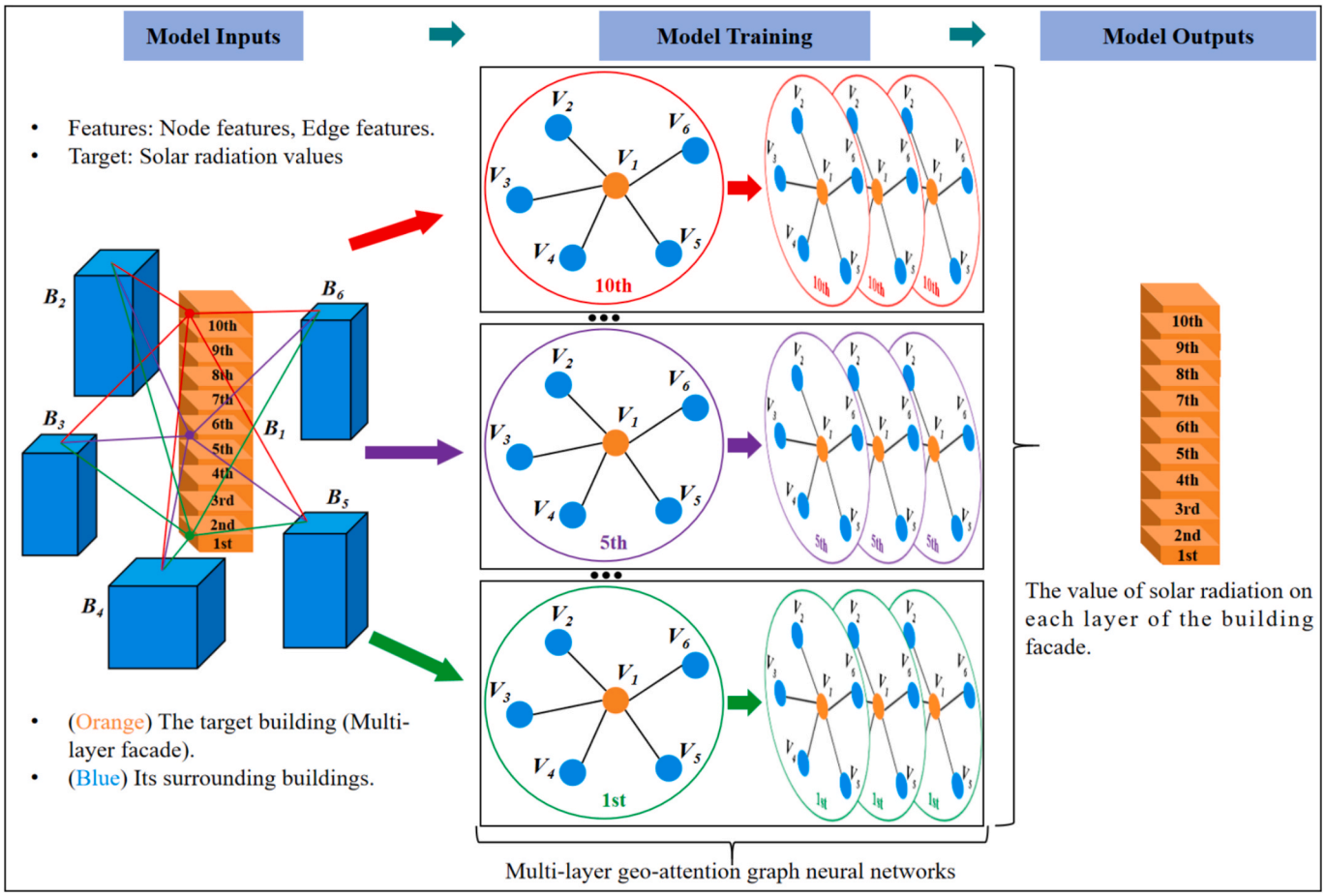

Fig. 7. The workflow of the MLGA-GNN model.

2.5. Estimation of PV power generation potential

To evaluate the actual PV power generation potential of building facades, it is necessary to convert the solar radiation values into expected electrical energy output. The conversion process can be calculated using Equation (6) [46]:

$$FPV_{potential} = PCE \times T_{period} \times SRI \times \eta \quad (6)$$

where the parameters are defined as follows:

- $FPV_{potential}$: expected PV power generation
- PCE: photoelectric conversion efficiency of the PV system
- T_{period}: cumulative time of solar radiation
- SRI: solar radiation intensity per unit of time
- η: system performance coefficient, used to consider the loss factors during long-term operation of the equipment

Based on existing research findings and practical application experience [47–49], this study adopts the following parameter settings:

- $PCE = 15$ % (photoelectric conversion efficiency)
- $T_{period} = 1$ year (annual cumulative power generation)
- $\eta = 90$ % (effective coefficient considering system losses)

2.6. Estimation of investment cost and carbon reduction

To assess the economic feasibility and environmental benefits of building facade PV systems, we constructed a comprehensive evaluation framework that calculates the SRI installation thresholds, net income, and carbon reduction under different payback period scenarios [50–52].

The calculation process utilized actual data from the NYC government and relevant departments, including average electricity prices ($0.1611/kWh) [53], PV system investment costs ($1.56/W) [54], and carbon emission factor (0.3705 kg/kWh) [55]. Considering the long-term performance degradation of PV systems, we assumed that from the 11th year onwards, the system efficiency would decrease to 80 % of its initial efficiency [56].

First, we determine the installation threshold for SRI using Equations (7) and (8). Equation (7) calculates the initial investment cost, and then Equation (8) is used to derive the minimum $\boldsymbol{SRI_{25}}$ required for a 25-year payback period. This threshold represents the minimum ***SRI*** needed for the investment to be exactly recouped within 25 years under given conditions: (***INV***: initial investment cost, $\boldsymbol{C_W}$: investment cost per watt of PV system, ***CAP***: PV system capacity).

$$INV = C_W * CAP \quad (7)$$

$$SRI_{25} = \frac{INV}{25 \times PCE \times T_{period} \times \eta * ER} \quad (8)$$

For installation locations that meet or exceed the $\boldsymbol{SRI_{25}}$ threshold, we further evaluate their economic benefits using Equations (9) and (10). Equation (9) calculates the annual cost savings (***ACS***), while Equation (10) considers the changes in benefits over different periods and computes the total net income over 25 years: (***ER***: electricity rate, $\boldsymbol{NI_{25}}$: net income over 25 years).

$$ACS = FPV_{potential} * ER \quad (9)$$

$$NI_{25} = ACS_{10} * 10 + ACS_{15} * 15 - INV \quad (10)$$

Finally, the environmental benefits are evaluated using Equation

(11), which calculates the total carbon emission reduction of these PV systems over their 25-year operational period: (***CR***: carbon reduction, ***CEF***: carbon emission factor).

$$CR = FPV_{potential} * CEF \tag{11}$$

2.7. Metrics for evaluating model performance

To evaluate model performance in predicting PV potential on building facades, this study employs two common standard evaluation metrics: root mean square error (RMSE) and R-squared (R^2) [57], with the calculation formulas shown in Equations (12) and (13). RMSE measures the prediction accuracy by calculating the average deviation between predicted and true values, with smaller values indicating lower prediction errors. R2, on the other hand, reflects the model's ability to explain data variability, ranging from 0 to 1, with values closer to 1 indicating better model fit and reflecting the correlation between predicted and actual values. These two metrics provide a systematic evaluation of the model's predictive performance from different perspectives.

$$RMSE = \sqrt{\frac{1}{n}\sum_{i=1}^{n}(y_i - \hat{y}_i)^2} \tag{12}$$

$$R^2 = 1 - \frac{\sum_{i=1}^{n}(y_i - \hat{y}i)^2}{\sum_{i=1}^{n}(y_i - \bar{y})^2} \tag{13}$$

where, n is the total number of samples, y_i is the actual solar radiation value of the i-th sample, $\hat{y}i$ is the predicted solar radiation value of the i-th sample, $\bar{y}$ is the mean value of all actual samples.

3. Results

3.1. Model prediction performance comparison

To validate the performance of the MLGA-GNN model, this study selected five representative models for comparison: machine learning models including Gradient Boosting Decision Tree (GBDT) [58], Random Forest [59], and Deep Neural Network (DNN) [60], and GNN models including Graph Convolutional Network (GCN) [61] and Graph Attention network (GAT) [62]. These models cover different types of learning methods and provide a comprehensive evaluation of the predictive performance of MLGA-GNN.

From the experimental results in Table 3, it can be observed that GNN-based models generally perform better than traditional machine learning methods, fully demonstrating the advantages of GNNs in predicting PV potential in buildings. Specifically:

GNNs vs. Traditional ML methods: Comparing GCN and GAT with traditional machine learning methods such as GBDT, Random Forest, and DNN, it is found that GNN-based models achieve better performance on all metrics. Taking RMSE as an example, the performance of GCN and GAT (0.8588 and 0.7998) is significantly better than that of GBDT, Random Forest, and DNN (1.0241, 0.9192, and 1.0820). This is mainly because GNNs can effectively utilize the topological relationships between buildings and incorporate the information of surrounding buildings into the feature representation of the target building. In contrast, traditional ML methods can only use the attribute features of individual buildings, ignoring the influence of the building environment.

GAT vs. GCN: Further comparing two mainstream GNN models, GAT outperforms GCN. This is due to the introduction of an attention mechanism in GAT when aggregating neighboring node information, allowing the model to adaptively assign importance to different neighbors and focus on surrounding buildings that have a greater association and stronger influence on the target building. For example, in terms of the R-squared metric for SRI, GAT achieves 0.6989, surpassing GCN's 0.6492.

MLGA-GNN vs. GAT: The proposed MLGA-GNN model achieves the best performance on all evaluation metrics, further improving the prediction performance. This is mainly attributed to the incorporation of rich geometric features (azimuth angle, pitch angle, and distance) into the attention computation, enabling the model to more comprehensively characterize the spatial relationships between buildings. For instance, the RMSE (0.7790) and R-squared (0.8833) of MLGA-GNN are both superior to those of GAT (0.7998 and 0.8623).

Table 3
Performance of different models on building facades.

	Solar radiation indicators	Radiation intensity		Total radiation	
	Metrics	RMSE	R-Squared	RMSE	R-Squared
Machine learning	GBDT	0.7404	0.5333	1.0241	0.7110
	Random forest	0.6518	0.6215	0.9192	0.7699
	DNN	0.7212	0.5352	1.0820	0.6759
GNNs	Graph Convolutional Network (GCN)	0.6316	0.6492	0.8588	0.8130
	Graph attention network (GAT)	0.5810	0.6989	0.7998	0.8623
	MLGA-GNN (our work)	0.5639	0.7219	0.7790	0.8833

3.2. Solar radiation distribution on facade layers

This study assesses the PV potential of building facades in NYC by analyzing the distribution of SRI. The research methodology involves uniformly dividing the facades of each building into 10 height layers and calculating the SRI at each level to generate 10 detailed spatial distribution maps (Fig. 8). The analysis results reveal significant spatial heterogeneity in solar radiation on building facades, which is mainly reflected in two dimensions:

In the horizontal direction, there are significant differences between different regions. Due to the high density of buildings and mutual shading, central urban areas generally receive lower SRI on their facades than peripheral areas with lower building density. It is worth noting that this horizontal difference becomes more pronounced with increasing height, mainly because the influence of shading from surrounding buildings gradually decreases at higher positions.

In the vertical direction, the SRI exhibits an increasing trend with increasing height. The lower levels of buildings experience the most significant shading effect from surrounding buildings, resulting in generally lower SRI. In contrast, the top levels are least affected by shading and more readily receive direct sunlight, resulting in the highest SRI. This vertical gradient feature is prevalent in various regions of NYC, but the degree of gradient may vary among different regions.

4. Discussion

4.1. Comparison to the traditional assessment method

To highlight the innovative value of this research, we compared the traditional evaluation method with the multi-layer evaluation method employed in this study. Fig. 9 clearly demonstrates the differences in evaluation results between the two methods, indicating that the traditional method may underestimate PV potential of building facades (The regional differences in the black circles are particularly pronounced). The traditional holistic evaluation method has significant limitations: it treats the entire facade as a single entity and calculates the average SRI, masking the vertical gradient of SRI, leading to an underestimation of the potential at the upper parts of buildings and an overestimation at the lower parts. Furthermore, in the traditional evaluation results, many buildings only exhibit moderate or low SRI (light red areas), and this averaging process may cause some local high-radiation areas (especially at the upper parts of buildings) to be overlooked. More importantly, such

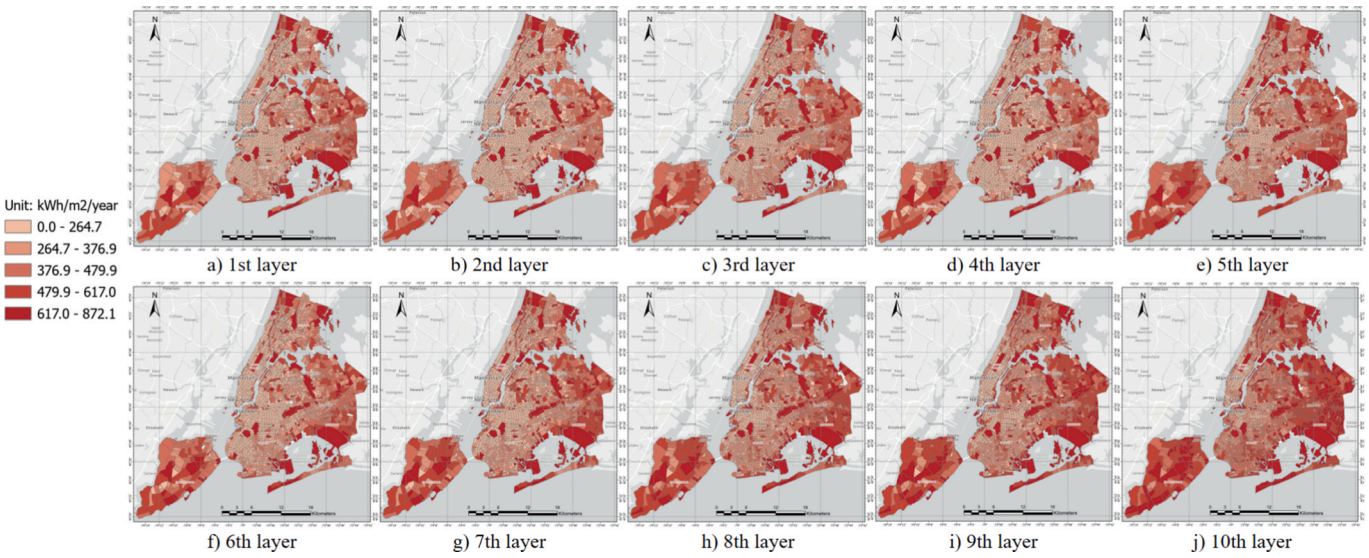

Fig. 8. Distribution of SRI on different building facade layers.

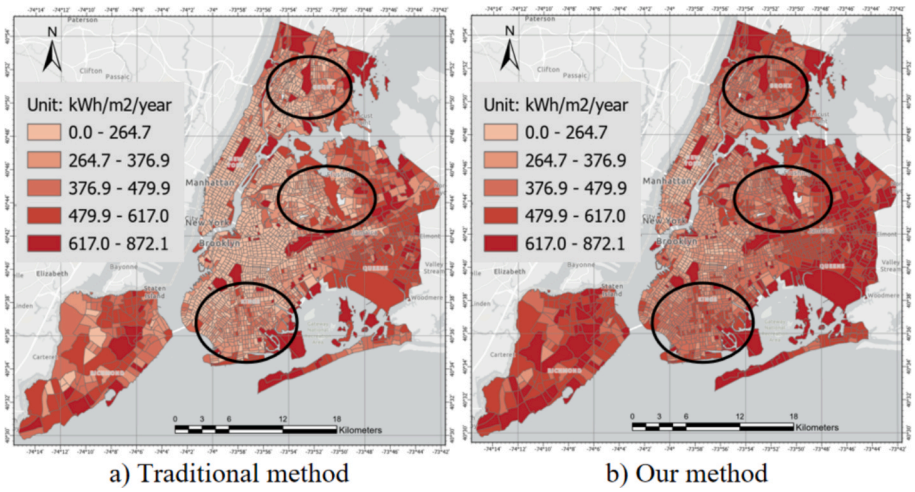

Fig. 9. Comparison of solar radiation distribution. (Note: our method is shown here only for the 10th layer, the full distribution is shown in Fig. 8).

averaging may mislead decision-makers' judgments, causing some buildings with good local solar exposure conditions to be excluded from PV development plans due to low overall scores.

In contrast, the multi-layer evaluation method proposed in this study has significant advantages: by evaluating in layers, it accurately reflects the variation of SRI along the vertical direction of building facades, particularly the high-radiation characteristics at the top layer, providing a more reliable basis for comprehensively assessing the PV potential of buildings. The results show that most building tops exhibit high SRI (red areas), which helps identify the most valuable areas for development and provides guidance for the optimal layout of PV systems. Based on the multi-layer evaluation results, more targeted development strategies can be formulated: prioritizing the deployment of PV systems in high-radiation areas (e.g., top layers) and adopting other energy-saving measures in low-radiation areas, thereby improving overall energy utilization efficiency.

This refined evaluation method not only improves the assessment accuracy but also provides more valuable insights for planning and designing building PV systems. By overcoming the limitations of traditional methods, the multi-layer evaluation method opens up new perspectives for assessing the PV potential of urban buildings, contributing to the scientific layout and efficient utilization of building PV systems.

4.2. Spatial heterogeneity analysis of solar radiation intensity

The findings in Fig. 8, reveal significant spatial heterogeneity in the distribution of solar energy resources on building facades in NYC, primarily in horizontal and vertical dimensions. In the horizontal dimension, central urban areas, due to high building density and tall structures, exhibit pronounced shading effects between buildings, resulting in lower SRI on facades. In contrast, peripheral urban areas have lower building density and larger spacing, reducing the shading effect and thus generally experiencing higher facade SRI. This horizontal difference directly reflects the influence of urban land use intensity and the built environment.

In the vertical dimension, the SRI on building facades increases with height, which is mainly related to the solar altitude angle and sky view factor. The lower levels of buildings are heavily shaded by surrounding buildings and ground features, resulting in the smallest sky view factor and, consequently, the lowest SRI. As height increases, the shading effect gradually weakens, and the sky view factor increases, allowing the facades to receive more direct solar radiation. It is worth noting that even in the central urban areas with overall lower SRI, the top facades of some high-rise buildings still exhibit high SRI, highlighting the importance of height advantage in solar energy resource acquisition.

These findings have guiding significance for optimizing building PV applications in NYC. Firstly, differentiated PV development strategies can be formulated: prioritizing the promotion of building-integrated PVs in areas with higher SRI, such as the urban periphery; for high-rise buildings in the central urban areas, customized PV system designs can be adopted for their top facades. This strategy helps maximize the economic benefits of PV systems while alleviating urban energy supply pressure. Secondly, the research results provide new ideas for urban planning and architectural design. For new buildings, shading effects can be minimized without compromising building density by optimizing parameters such as layout, spacing, height, and orientation; for existing buildings, targeted PV renovation plans can be developed based on the SRI distribution of their respective regions.

4.3. Vertical distribution differences of solar resources on building facades

To further quantify the vertical differences in solar radiation on building facades, we calculated the difference in SRI between the tenth layer (near the roof) and the first layer (near the ground) of each building based on the aforementioned facade layering results (Fig. 8), generating a vertical difference distribution map (Fig. 10). The results show that the range of difference values is 0–473.7 kWh/m^2, with an average value of 157.5 kWh/m^2. Considering the solar conditions in NYC, this vertical difference is highly significant, further confirming the necessity of a refined evaluation method.

From a spatial distribution perspective, areas with larger difference values are mainly concentrated in northern Manhattan, southern Brooklyn, and southern Queens (red circled areas in Fig. 10(c)). This finding is somewhat unexpected, as these areas have lower building density and height than central Manhattan. A possible explanation for this phenomenon is that due to severe shading effects in central Manhattan, building facades exhibit lower SRI from the bottom to the top layers, resulting in relatively smaller vertical differences. This result reveals the complexity of the formation mechanism of vertical differences in solar radiation on building facades and suggests the need for more in-depth research on the formation mechanisms of radiation distribution in different regions.

The vertical difference distribution map not only highlights the SRI differences between the top and bottom layers of building facades but also quantitatively describes the magnitude of these differences. For areas with larger difference values, the top layers of their building facades often have higher SRI, indicating that these areas have good potential for PV installation. This further proves that when assessing the PV potential of urban building facades, adopting a refined evaluation method can more accurately and efficiently identify high-potential areas, thereby improving the utilization efficiency of PV resources in urban vertical spaces.

These findings have significant implications for the planning and design of urban PV systems. The identification of vertical differences in SRI across building facades enables a more nuanced and location-specific deployment strategy. At the macro level, areas exhibiting high vertical SRI gradients can be identified as priority zones for PV system development. Urban planners can leverage this information to concentrate PV infrastructure in high-irradiance districts, thereby enhancing the overall energy yield of urban areas. At the micro level, the refined SRI data supports facade-level design decisions. For instance, in buildings located in high-gradient zones, PV panels should be preferentially installed on upper façade layers where solar exposure is greatest. Conversely, in areas with relatively uniform SRI distribution, other factors—such as architectural form, shading from adjacent structures, or aesthetic considerations—may play a more prominent role in determining the optimal PV configuration. This differentiated and data-informed strategy not only improves the efficiency of solar energy utilization on building facades but also aligns with broader sustainable urban development goals. It supports the creation of adaptable energy systems that are tailored to the specific spatial and environmental characteristics of each urban context.

4.4. Cost-benefit and carbon reduction analysis

This study systematically assessed the economic feasibility and environmental benefits of building facade PV systems. Table 4 presents the analysis results under different payback period scenarios, ranging from 5 to 25 years, including the required minimum SRI thresholds, economic benefits (net income), and environmental benefits (carbon reduction). The analysis revealed a clear inverse relationship between the payback period and the SRI threshold. As the payback period shortened from 25 to 5 years, the required minimum SRI increased from 329.2 to 1448.4 kWh/m^2/year, indicating that shorter payback periods demand better solar conditions.

The results showed a positive correlation between the payback period and system benefits. Taking the 25-year period as an example, installing PV systems on facades that meet the minimum SRI

Table 4
The results of cost benefits and carbon reduction.

Payback period (year)	Threshold of SRI (kWh/m2/year)	Net income (billion $)	Carbon reduction (million tons)
25	329.2	39.6	238.0
20	402.3	38.1	204.5
15	517.3	31.0	146.4
10	724.2	7.2	29.0
5	1448.4	0.0	0

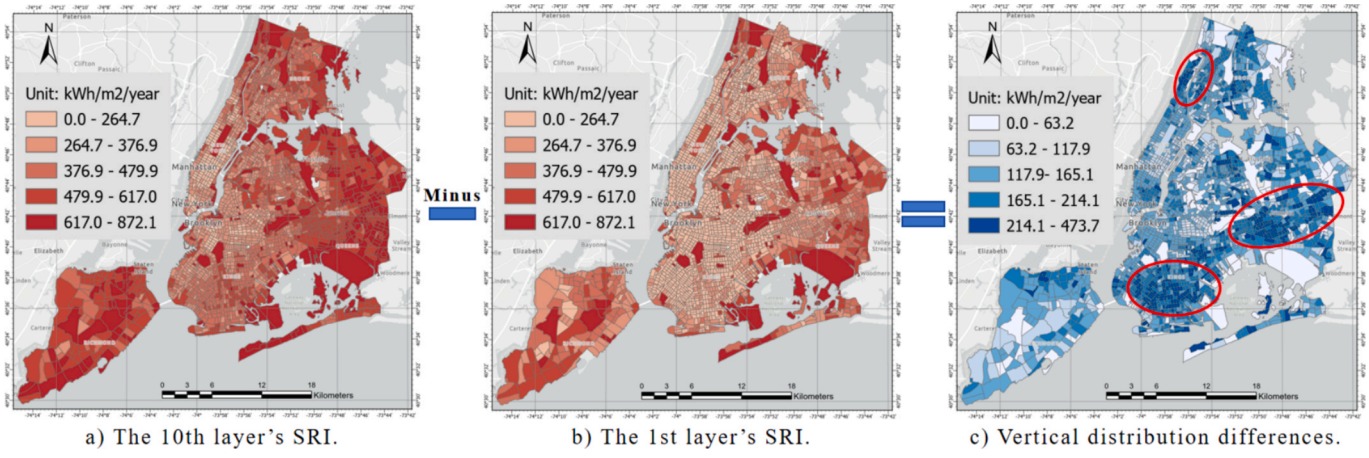

a) The 10th layer's SRI. b) The 1st layer's SRI. c) Vertical distribution differences.

Fig. 10. The map of vertical differences of solar radiation on building facades.

requirement ($\geq$329.2 kWh/m^2/year) can achieve a net income of $39.6 billion and a carbon reduction of 238 million tons. This demonstrates that extending the payback period reduces capital turnover efficiency but can generate greater long-term economic and environmental benefits.

In practical applications, it is necessary to weigh the advantages and disadvantages of different investment periods. While the 25-year plan yields the highest overall benefits, it requires significant initial capital pressure. The 10–15-year medium-term plans offer a more balanced performance in terms of benefits and SRI requirements. For instance, the 10-year plan can already achieve a carbon reduction of 29 million tons, making it a potentially ideal choice. The 5-year plan, on the other hand, is more suitable for projects seeking rapid investment returns but requires higher installation conditions.

This analysis provides valuable guidance for formulating differentiated PV development strategies. Investors can choose suitable building facades based on their objectives: projects pursuing quick returns prioritize high SRI areas, while projects focusing on long-term benefits can cover a wider range. Policymakers can develop targeted incentive measures based on local conditions, including solar energy resources, electricity price levels, and environmental protection goals, to promote the rational layout and optimal configuration of PV systems.

4.5. Limitations and future work

The MLGA-GNN model proposed in this study is innovative in predicting building PV potential, but there is still room for optimization in the definition of building graph data. Currently, the model simplifies all relationships between buildings into an undirected graph structure, assuming mutual influence among buildings. Although this simplification reduces modeling complexity, it does not fully reflect real-world conditions. In practice, the influence between buildings is often asymmetric. A typical example is that the shading effect of high-rise buildings on surrounding low-rise buildings is significant, while the influence of low-rise buildings on high-rise buildings can be ignored. To address this simplification, we introduced three parameters to adjust the geo-attention coefficients. However, this compensatory measure still cannot fully overcome the limitations of the undirected graph representation, which may affect the model's prediction accuracy. With the advancement of high-performance computing technology, future research can consider adopting a directed graph structure to more accurately represent the asymmetric relationships between buildings. This improvement not only enables a more realistic reflection of the mutual influence between buildings but also has the potential to further enhance the model's predictive performance.

5. Conclusion

This study proposes an innovative MLGA-GNN model for assessing the PV potential of urban building facades. By vertically stratifying building facades and incorporating a geospatial attention mechanism, the model can more accurately capture the spatial distribution of SRI on building facades. Experimental results on 1.08 million buildings in NYC demonstrate that the MLGA-GNN model significantly outperforms traditional machine learning methods and basic GNN models in terms of prediction accuracy. By introducing the geospatial attention mechanism, the model better portrays the complex spatial relationships among building clusters.

Compared to traditional evaluation methods, the stratified evaluation approach in this study has significant advantages. The averaging approach of traditional methods may overlook some local high-radiation areas (especially on the upper parts of buildings), excluding buildings with good local solar conditions from PV development plans due to their lower overall scores. In contrast, the stratified method in this study not only accurately reflects the variations of SRI along the vertical direction of building facades but also provides a more reliable basis for optimizing the layout of PV systems.

Moreover, the SRI on building facades exhibits significant heterogeneity in spatial distribution. Horizontally, due to differences in building density, the SRI received by facades in central areas like Manhattan is generally lower than that in surrounding areas such as Brooklyn and Queens. Vertically, the SRI shows an increasing trend with height, with the difference between the top and bottom layers reaching up to 473.7k Wh/m^2. The spatial distribution of this vertical difference varies significantly across different regions, fully reflecting the profound impact of NYC's complex urban morphology on the distribution of solar energy resources.

Economic and environmental benefit analyses indicate that the payback period is inversely related to the SRI threshold, with a 5-year payback period requiring a minimum SRI of 1448.4 kWh/m^2/year. In the long run, the 25-year plan can achieve a net income of $39.6 billion and a carbon reduction of 238 million tons, demonstrating significant economic and environmental benefits. The 10–15-year medium-term plans achieve a balance between benefits and costs, making them potentially more suitable choices for practical applications. These findings provide important decision-making references for promoting building PV projects in NYC.

The research findings have important practical implications for urban PV development. Based on the results from NYC, a typical global high-density city, this study provides a scientific basis for planning urban PV systems and supports the formulation of differentiated development strategies. By accurately identifying high-potential areas on building facades, it can guide the optimal layout of building PV systems and improve the utilization efficiency of solar energy resources. These findings offer viable paths for achieving low-carbon transformation in the building sector.

CRediT authorship contribution statement

Zheng Li: Writing – original draft, Visualization, Validation, Software, Methodology, Formal analysis, Data curation, Conceptualization. **Jun Ma:** Writing – review & editing, Supervision, Resources, Project administration, Investigation, Funding acquisition. **Waishan Qiu:** Writing – review & editing, Validation, Investigation. **Xiao Li:** Writing – review & editing, Validation, Resources. **Feifeng Jiang:** Writing – review & editing, Visualization, Supervision, Resources.

Declaration of competing interest

The authors declare that they have no known competing financial interests or personal relationships that could have appeared to influence the work reported in this paper.

Acknowledgments

This study was jointly supported by the Early Career Scheme (No. 27202521) from the Hong Kong Research Grants Council and the Seed Fund for PI Research – Basic Research (No. 2202100879) from the University of Hong Kong. We would like to express our sincere gratitude for their support.

Data availability

Data will be made available on request.

References

[1] 2022 Global Status Report for Buildings and Construction, UNEP - UN Environment Programme (2022). http://www.unep.org/resources/publication/2022-global-status-report-buildings-and-construction.
[2] Y. Wang, D. Mauree, Q. Sun, H. Lin, J.L. Scartezzini, R. Wennersten, A review of approaches to low-carbon transition of high-rise residential buildings in China,

Renew. Sustain. Energy Rev. 131 (2020) 109990, https://doi.org/10.1016/j.rser.2020.109990.
[3] F. Huide, Z. Xuxin, M. Lei, Z. Tao, W. Qixing, S. Hongyuan, A comparative study on three types of solar utilization technologies for buildings: Photovoltaic, solar thermal and hybrid photovoltaic/thermal systems, Energ. Conver. Manage. 140 (2017) 1–13, https://doi.org/10.1016/j.enconman.2017.02.059.
[4] Z. Li, J. Ma, Y. Tan, C. Guo, X. Li, Combining physical approaches with deep learning techniques for urban building energy modeling: A comprehensive review and future research prospects, Build. Environ. 246 (2023) 110960, https://doi.org/10.1016/j.buildenv.2023.110960.
[5] Z. Liu, Z. Guo, Q. Chen, C. Song, W. Shang, M. Yuan, H. Zhang, A review of data-driven smart building-integrated photovoltaic systems: Challenges and objectives, Energy 263 (2023) 126082, https://doi.org/10.1016/j.energy.2022.126082.
[6] W. Wang, H. Yang, C. Xiang, Green roofs and facades with integrated photovoltaic system for zero energy eco-friendly building – A review, Sustainable Energy Technol. Assess. 60 (2023) 103426, https://doi.org/10.1016/j.seta.2023.103426.
[7] A. Ramos, J. Romaní, J. Salom, Impact of building integrated photovoltaics on high rise office building in the Mediterranean, Energy Rep. 10 (2023) 3197–3210, https://doi.org/10.1016/j.egyr.2023.09.178.
[8] B. Svetozarevic, M. Begle, P. Jayathissa, S. Caranovic, R.F. Shepherd, Z. Nagy, I. Hischier, J. Hofer, A. Schlueter, Dynamic photovoltaic building envelopes for adaptive energy and comfort management, Nat. Energy 4 (2019) 671–682, https://doi.org/10.1038/s41560-019-0424-0.
[9] A. Vulkan, I. Kloog, M. Dorman, E. Erell, Modeling the potential for PV installation in residential buildings in dense urban areas, Energ. Buildings 169 (2018) 97–109, https://doi.org/10.1016/j.enbuild.2018.03.052.
[10] J. Esclapés, I. Ferreiro, J. Piera, J. Teller, A method to evaluate the adaptability of photovoltaic energy on urban façades, Sol. Energy 105 (2014) 414–427, https://doi.org/10.1016/j.solener.2014.03.012.
[11] M.E. Abdalazeem, H. Hassan, T. Asawa, H. Mahmoud, Review on integrated photovoltaic-green roof solutions on urban and energy-efficient buildings in hot climate, Sustain. Cities Soc. 82 (2022) 103919, https://doi.org/10.1016/j.scs.2022.103919.
[12] A. Saleh, N. Saleh, O. Ali, R. Hasan, O. Ahmed, A. Alias, K. Yassin, Green Building Techniques: Under the umbrella of the climate framework agreement, Babylonian Journal of Machine Learning 2024 (2024) 1–14, https://doi.org/10.58496/BJML/2024/001.
[13] D.F.Y. Mustafa, Daylighting in high-rise office buildings: A comprehensive review, KHWARIZMIA 2024 (2024) 74–84, https://doi.org/10.70470/KHWARIZMIA/2024/011.
[14] A.A.M. Yasser, Sustainable design strategies in architectural engineering: A comprehensive review, KHWARIZMIA 2025 (2025) 1–11, https://doi.org/10.70470/KHWARIZMIA/2025/001.
[15] K.R. Abdulkareem, E. Sonmez, Architectural Harmony with Nature, KHWARIZMIA 2024 (2024) 4–7, https://doi.org/10.70470/KHWARIZMIA/2024/002.
[16] S. Izquierdo, M. Rodrigues, N. Fueyo, A method for estimating the geographical distribution of the available roof surface area for large-scale photovoltaic energy-potential evaluations, Sol. Energy 82 (2008) 929–939.
[17] J. Ordóñez, E. Jadraque, J. Alegre, G. Martínez, Analysis of the photovoltaic solar energy capacity of residential rooftops in Andalusia (Spain), Renew. Sustain. Energy Rev. 14 (2010) 2122–2130, https://doi.org/10.1016/j.rser.2010.01.001.
[18] L.K. Wiginton, H.T. Nguyen, J.M. Pearce, Quantifying rooftop solar photovoltaic potential for regional renewable energy policy, Comput. Environ. Urban Syst. 34 (2010) 345–357, https://doi.org/10.1016/j.compenvurbsys.2010.01.001.
[19] R. Singh, R. Banerjee, Estimation of rooftop solar photovoltaic potential of a city, Sol. Energy 115 (2015) 589–602, https://doi.org/10.1016/j.solener.2015.03.016.
[20] Q. Li, S. Krapf, L. Mou, Y. Shi, X.X. Zhu, Deep learning-based framework for city-scale rooftop solar potential estimation by considering roof superstructures, Appl. Energy 374 (2024) 123839.
[21] H. Mao, X. Chen, Y. Luo, J. Deng, Z. Tian, J. Yu, Y. Xiao, J. Fan, Advances and prospects on estimating solar photovoltaic installation capacity and potential based on satellite and aerial images, Renew. Sustain. Energy Rev. 179 (2023) 113276.
[22] J. Yang, J. Wu, J. Lu, X. Peng, H. Yuan, L.L. Lai, A novel method for assessment rooftop PV potential based on remote sensing images, Renew. Energy 237 (2024) 121810.
[23] T. Zhong, Z. Zhang, M. Chen, K. Zhang, Z. Zhou, R. Zhu, Y. Wang, G. Lü, J. Yan, A city-scale estimation of rooftop solar photovoltaic potential based on deep learning, Appl. Energy 298 (2021) 117132, https://doi.org/10.1016/j.apenergy.2021.117132.
[24] C. Catita, P. Redweik, J. Pereira, M.C. Brito, Extending solar potential analysis in buildings to vertical facades, Comput. Geosci. 66 (2014) 1–12, https://doi.org/10.1016/j.cageo.2014.01.002.
[25] G. Mangherini, V. Diolaiti, P. Bernardoni, A. Andreoli, D. Vincenzi, Review of façade photovoltaic solutions for less energy-hungry buildings, Energies 16 (2023) 6901, https://doi.org/10.3390/en16196901.
[26] W.L. Schram, E. Shirazi, PV on façades: A financial, technical and environmental assessment, Energ. Buildings 328 (2025) 115010.
[27] F. Vahdatikhaki, M.V. Barus, Q. Shen, H. Voordijk, A. Hammad, Surrogate modelling of solar radiation potential for the design of PV module layout on entire façade of tall buildings, Energ. Buildings 286 (2023) 112958.
[28] J. Čurpek, M. Čekon, Building performance simulation of a photovoltaic façade enhanced with latent heat storage: Model validation and power generation prediction, J. Storage Mater. 56 (2022) 106143.
[29] M. Karteris, I. Theodoridou, G. Mallinis, A.M. Papadopoulos, Façade photovoltaic systems on multifamily buildings: An urban scale evaluation analysis using geographical information systems, Renew. Sustain. Energy Rev. 39 (2014) 912–933.
[30] M.C. Brito, S. Freitas, S. Guimarães, C. Catita, P. Redweik, The importance of facades for the solar PV potential of a Mediterranean city using LiDAR data, Renew. Energy 111 (2017) 85–94, https://doi.org/10.1016/j.renene.2017.03.085.
[31] J. Liu, Q. Wu, Z. Lin, H. Shi, S. Wen, Q. Wu, J. Zhang, C. Peng, A novel approach for assessing rooftop-and-facade solar photovoltaic potential in rural areas using three-dimensional (3D) building models constructed with GIS, Energy 282 (2023) 128920, https://doi.org/10.1016/j.energy.2023.128920.
[32] L. Tao, M. Wang, C. Xiang, Assessing urban morphology's impact on solar potential of high-rise facades in Hong Kong using machine learning: An application for FIPV optimization, Sustain. Cities Soc. 117 (2024) 105978, https://doi.org/10.1016/j.scs.2024.105978.
[33] M.S. Roudsari, M. Pak, Ladybug: a parametric environmental plugin for grasshopper to help designers create an environmentally-conscious design, (2013). https://www.aivc.org/resource/ladybug-parametric-environmental-plugin-grasshopper-help-designers-create-environmentally.
[34] J. de Sousa Freitas, J. Cronemberger, R.M. Soares, C.N.D. Amorim, Modeling and assessing BIPV envelopes using parametric Rhinoceros plugins Grasshopper and Ladybug, Renew. Energy 160 (2020) 1468–1479.
[35] N. Bushra, A comprehensive analysis of parametric design approaches for solar integration with buildings: A literature review, Renew. Sustain. Energy Rev. 168 (2022) 112849.
[36] U. Jamil, T. Hickey, J.M. Pearce, Solar energy modelling and proposed crops for different types of agrivoltaics systems, Energy 304 (2024) 132074, https://doi.org/10.1016/j.energy.2024.132074.
[37] Y. Hu, X. Cheng, S. Wang, J. Chen, T. Zhao, E. Dai, Times series forecasting for urban building energy consumption based on graph convolutional network, Appl. Energy 307 (2022) 118231, https://doi.org/10.1016/j.apenergy.2021.118231.
[38] Z. Li, J. Ma, F. Jiang, S. Zhang, Y. Tan, Assessing the impacts of urban morphological factors on urban building energy modeling based on spatial proximity analysis and explainable machine learning, J. Build. Eng. 85 (2024) 108675, https://doi.org/10.1016/j.jobe.2024.108675.
[39] Z. Li, J. Ma, F. Jiang, Exploring the effects of 2D/3D building factors on urban energy consumption using explainable machine learning, J. Build. Eng. 97 (2024) 110827, https://doi.org/10.1016/j.jobe.2024.110827.
[40] P. Cui, J. Lu, Y. Wu, J. Tang, J. Jiang, Effect of urban morphology on microclimate and building cluster energy consumption in cold regions of China, Sustain. Cities Soc. 115 (2024) 105838, https://doi.org/10.1016/j.scs.2024.105838.
[41] A. Kamal, S.M.H. Abidi, A. Mahfouz, S. Kadam, A. Rahman, I.G. Hassan, L.L. Wang, Impact of urban morphology on urban microclimate and building energy loads, Energ. Buildings 253 (2021) 111499, https://doi.org/10.1016/j.enbuild.2021.111499.
[42] H. Zhao, C. Liu, R. Jing Yang, C. Sun, Large-scale prediction of solar irradiation, shading impacts, and energy generation on building Façade through urban morphological indicators: A machine learning approach, Energy Build 323 (2024) 114797, https://doi.org/10.1016/j.enbuild.2024.114797.
[43] S. Wettewa, L. Hou, G. Zhang, Graph Neural Networks for building and civil infrastructure operation and maintenance enhancement, Adv. Eng. Inf. 62 (2024) 102868, https://doi.org/10.1016/j.aei.2024.102868.
[44] B. Lei, P. Liu, N. Milojevic-Dupont, F. Biljecki, Predicting building characteristics at urban scale using graph neural networks and street-level context, Comput. Environ. Urban Syst. 111 (2024) 102129, https://doi.org/10.1016/j.compenvurbsys.2024.102129.
[45] B. Kong, T. Ai, X. Zou, X. Yan, M. Yang, A graph-based neural network approach to integrate multi-source data for urban building function classification, Comput. Environ. Urban Syst. 110 (2024) 102094, https://doi.org/10.1016/j.compenvurbsys.2024.102094.
[46] Y. Zhang, J. Ren, Y. Pu, P. Wang, Solar energy potential assessment: A framework to integrate geographic, technological, and economic indices for a potential analysis, Renew. Energy 149 (2020) 577–586, https://doi.org/10.1016/j.renene.2019.12.071.
[47] L. Cheng, F. Zhang, S. Li, J. Mao, H. Xu, W. Ju, X. Liu, J. Wu, K. Min, X. Zhang, M. Li, Solar energy potential of urban buildings in 10 cities of China, Energy 196 (2020) 117038, https://doi.org/10.1016/j.energy.2020.117038.
[48] B. Petter Jelle, C. Breivik, H. Drolsum Røkenes, Building integrated photovoltaic products: A state-of-the-art review and future research opportunities, Solar Energy Mater. Solar Cells 100 (2012) 69–96, https://doi.org/10.1016/j.solmat.2011.12.016.
[49] G. Li, G. Wang, T. Luo, Y. Hu, S. Wu, G. Gong, C. Song, Z. Guo, Z. Liu, SolarSAM: Building-scale photovoltaic potential assessment based on Segment Anything Model (SAM) and remote sensing for emerging city, Renew. Energy 237 (2024) 121560, https://doi.org/10.1016/j.renene.2024.121560.
[50] L. Yan, R. Zhu, M.-P. Kwan, W. Luo, D. Wang, S. Zhang, M.S. Wong, L. You, B. Yang, B. Chen, L. Feng, Estimation of urban-scale photovoltaic potential: A deep learning-based approach for constructing three-dimensional building models from optical remote sensing imagery, Sustain. Cities Soc. 93 (2023) 104515, https://doi.org/10.1016/j.scs.2023.104515.
[51] T. Chen, N. Zhang, Z. Ye, K. Jiang, Z. Lin, H. Zhang, Y. Xu, Q. Liu, H. Huang, Carbon reduction benefits of photovoltaic-green roofs and their climate change mitigation potential: A case study of Xiamen city, Sustain. Cities Soc. 114 (2024) 105760, https://doi.org/10.1016/j.scs.2024.105760.
[52] Z. Zhang, M. Chen, T. Zhong, R. Zhu, Z. Qian, F. Zhang, Y. Yang, K. Zhang, P. Santi, K. Wang, Y. Pu, L. Tian, G. Lü, J. Yan, Carbon mitigation potential afforded by rooftop photovoltaic in China, Nat. Commun. 14 (2023) 2347, https://doi.org/10.1038/s41467-023-38079-3.

[53] Electricity Data - U.S. Energy Information Administration (EIA), (n.d.). https://www.eia.gov/electricity/data.php.
[54] V. Ramasamy, D. Feldman, J. Desai, R. Margolis, U.S. Solar Photovoltaic System and Energy Storage Cost Benchmarks: Q1 2021, National Renewable Energy Lab. (NREL), Golden, CO (United States), 2021. https://doi.org/10.2172/1829460.
[55] O. US EPA, Emissions & Generation Resource Integrated Database (eGRID), (2020). https://www.epa.gov/egrid.
[56] X. Zhou, Z. Huang, B. Scheuer, W. Lu, G. Zhou, Y. Liu, High-resolution spatial assessment of the zero energy potential of buildings with photovoltaic systems at the city level, Sustain. Cities Soc. 93 (2023) 104526, https://doi.org/10.1016/j.scs.2023.104526.
[57] Z. Li, J. Ma, Q. Wang, M. Wang, F. Jiang, Enhancing urban solar irradiation prediction with shadow-attention graph neural networks: Implications for net-zero energy buildings in New York City, Sustain. Cities Soc. 120 (2025) 106133, https://doi.org/10.1016/j.scs.2025.106133.
[58] J. Son, I. Jung, K. Park, B. Han, Tracking-by-segmentation with online gradient boosting decision tree, in: Proceedings of the IEEE International Conference on Computer Vision, 2015: pp. 3056–3064.
[59] G. Biau, E. Scornet, A random forest guided tour, TEST 25 (2016) 197–227.
[60] V. Sze, Y.-H. Chen, T.-J. Yang, J.S. Emer, Efficient processing of deep neural networks: A tutorial and survey, Proc. IEEE 105 (2017) 2295–2329.
[61] A. Fout, J. Byrd, B. Shariat, A. Ben-Hur, Protein Interface Prediction using Graph Convolutional Networks, in: Advances in Neural Information Processing Systems, Curran Associates, Inc., 2017. https://proceedings.neurips.cc/paper/2017/hash/f507783927f2ec2737ba40afbd17efb5-Abstract.html.
[62] S. Brody, U. Alon, E. Yahav, How Attentive are Graph Attention Networks?, (2022). http://arxiv.org/abs/2105.14491.